sustainability

MDPI

Article

Monitoring the Performance and Sustainability Impact of a Balcony-Mounted Photovoltaic System with Battery Storage in Northern Italy

Stefano Rampino [1,*], Antonino Laudani [2], Gabriele Maria Lozito [1,3] and Francesco Pattini [1,*]

[1] Consiglio Nazionale delle Ricerche, IMEM Institute, 43124 Parma, Italy; gabrielemaria.lozito@unifi.it
[2] Department of Electrical Electronic and Computer Engineering, University of Catania, 95125 Catania, Italy; alaudani@unict.it
[3] Department of Information Engineering, University of Florence, Via di Santa Marta 3, 50139 Firenze, Italy
* Correspondence: stefano.rampino@cnr.it (S.R.); francesco.pattini@cnr.it (F.P.)

Abstract

This study presents a full year of continuous field monitoring of a balcony-mounted photovoltaic system with battery energy storage (PV-BESS) operating in zero feed-in mode near Parma, Italy. The 1.38 kWp array (60° tilt) was coupled to a 6 kW hybrid inverter and a 2.56 kWh $LiFePO_4$ battery to shift daytime solar surplus toward the evening demand peak. The system achieved an average annual Self-Sufficiency Ratio (SSR) of 32.3% (55.8% in summer), while zero feed-in curtailment removed 16.4% of the theoretical yield. An unexpected finding, termed the Appliance Paradox, reveals that in deep winter the inverter's standby consumption exceeded the scarce PV yield, turning winter SSR negative (−10.6%). A novel Energy Advantage Index (EAI) is introduced as a PV-BESS design figure of merit, predicting the optimal deactivation window and, prospectively, sizing inverter pairings to avoid the paradox. Economically, a CAPEX of about €1100 yields a 4.6-year payback and a ten-year ROI of about 137%, improving to 4.3 years and 154% under EAI-driven seasonal control, while cutting the effective cost of electricity by 28% and avoiding 2.35 t CO_2eq over ten years. Balcony PV-BESS systems can meaningfully advance residential energy autonomy, provided inverter sizing and seasonal operation are managed proactively. By jointly quantifying its technical, economic, social and environmental dimensions, this work provides a replicable sustainability assessment framework for residential balcony PV-BESS deployment.

Keywords: balcony PV; appliance paradox; plug-and-play (P&P); PV monitoring; energy democracy and sustainability; zero feed-in

Check for updates

Academic Editors: Francesco Calise, Maria Vicidomini, Rafał Figaj and Francesco Liberato Cappiello

Received: 13 October 2026
Revised: 9 November 2026
Accepted: 11 November 2026
Published: 13 November 2026

Copyright: © 2026 by the authors. Licensee MDPI, Basel, Switzerland. This article is an open access article distributed under the terms and conditions of the Creative Commons Attribution (CC BY) license.

1. Introduction

The transition towards decentralized renewable energy generation has accelerated the adoption of residential photovoltaic (PV) systems [1], with distributed applications expected to account for nearly 40% of new global solar capacity additions through 2030. While traditional rooftop PV installations are widespread, their application in multi-dwelling buildings remains limited due to space constraints and ownership barriers. Consequently, balcony-mounted PV systems have rapidly expanded within the residential market, offering a viable solution for apartment residents to participate in the energy transition. In Germany alone, 435,000 new plug-in balcony PV systems were registered in 2024, a 41% year-on-year increase, pushing the national registered stock past one million units by mid-2025 [2].

Uptake is not confined to Europe: in the United States, plug-in distributed energy resources are spreading rapidly on the strength of their technical performance, despite substantial regulatory and permitting barriers that remain the primary obstacle to wider adoption [3]. Historically, the balcony PV market has been dominated by low-power, "plug-and-play" systems. However, these systems face a significant limitation: typically only around 45% of the PV energy produced is actually consumed on-site, while the remainder is fed back into the grid for little to no financial return under current regulatory frameworks [4]. This shortfall arises because peak solar generation rarely aligns with peak domestic load, which typically occurs in the early morning and evening [5]. To overcome the limitations of standard plug-and-play systems, this study investigates the integration of a Battery Energy Storage System (BESS). By coupling high-efficiency PV modules with a zero-feed-in hybrid inverter and a lithium-iron-phosphate ($LiFePO_4$) battery, it becomes possible to shift the solar energy generated during the day to the evening peak hours. $LiFePO_4$ chemistry is itself an active area of materials-level research, for example through DNA-directed fabrication of $LiFePO_4$ micro-roses aimed at high-performance electrodes [6]; the present study instead addresses the system level, i.e., the operation of a commercial $LiFePO_4$ battery within a zero-feed-in balcony PV-BESS. A recent study on residential BESS coupled with balcony PV in Korean apartment buildings similarly tested several operating modes and found that prioritizing PV power to charge the battery, with grid power used only as a fallback near full discharge, most effectively avoids battery depletion while maximizing self-consumption [7]. A field study of a load-controlled balcony PV battery storage prototype, tested under real conditions for a full year in Germany, similarly found that self-consumption without storage is often significantly below expectations, and that regulating battery charge and discharge to follow the household load can raise self-consumption to as much as 100% [8]. More broadly, uncertainty-aware optimization approaches are being developed for the management of renewable energy units in microgrids, for example in networks coupling hydrogen-powered vehicles and microgrids [9]; the present study instead follows an empirical, single-site monitoring approach, in which the variability of the solar resource and of the operating conditions is characterized by measurement rather than handled through a formal uncertainty-aware optimization layer. Recent studies on balcony PV have addressed the solar potential and the tilt of balcony installations by simulation, without storage [10–12], the integration of balcony power plants into smart-home systems [13] and, for systems with batteries, predictive and rule-based energy management [14,15] and the efficiency of the power-conversion topology [16]. For PV-battery systems in general, an analysis of emerging performance issues showed that power-electronics conversion losses and standby consumption, which is drawn from the grid when the battery is empty, substantially reduce the performance of home storage, conversion efficiency dropping sharply below about 20% of the nominal power [17]. These studies concern simulated yields, control strategies, hardware topologies or generic home storage systems; to the best of our knowledge, a complete year of measured data from a zero-feed-in balcony PV-BESS, quantifying how the standby and part-load losses of the inverter translate into a seasonal energy penalty and relating it to an operating criterion, is not available in the literature reviewed here. The present paper exhibits a comprehensive performance analysis based on a full year of experimental data from a balcony-mounted PV-BESS system located in Northern Italy, evaluating its impact on residential energy autonomy and self-consumption.

The original contributions of this study are the year-long, daily resolved dataset of a zero-feed-in balcony PV-BESS with measured load, PV generation, grid draw and irradiance (provided as Supplementary Materials); the identification and quantification of the Appliance Paradox, the winter regime in which the system draws more energy from the grid than it would without the PV-BESS; the Energy Advantage Index (EAI) as a

seasonal-deactivation and inverter-sizing criterion; the analysis of the curtailment ("clipping") imposed by zero feed-in operation; and an integrated technical, economic, social and environmental assessment.

2. Materials and Methods

2.1. System Configuration

The experimental setup was deployed on a residential balcony located 5 m above ground level (44.7824° N, 10.3107° E) in the Emilia-Romagna region (Northern Italy), an area characterized by the typical climatic conditions of the Po Valley. Table 1 reports the average monthly maximum and minimum air temperatures and the mean daily global horizontal irradiation recorded over the monitoring period [18], illustrating the seasonal range of atmospheric conditions to which the system was exposed.

Table 1. Average monthly maximum and minimum ambient temperatures and mean daily global horizontal irradiation (GHI; Vevor YT60234 horizontal sensor; May 2025: 8–31 May only) over the 365-day monitoring period.

Month and Year	Average Maximum Temperature (°C)	Average Minimum Temperature (°C)	Mean Daily Global Horizontal Irradiation (kWh/m^2/day)
May 2025	22	11	5.64
June 2025	28	16	6.32
July 2025	31	18	5.76
August 2025	31	19	4.88
September 2025	26	14	3.87
October 2025	19	10	2.54
November 2025	13	6	1.46
December 2025	8	2	0.86
January 2026	7	1	0.96
February 2026	10	2	1.99
March 2026	14	5	3.15
April 2026	18	8	4.70
Annual average	18.9	9.3	3.51

The system architecture consists of a photovoltaic array, a hybrid inverter, a battery energy storage system (BESS), and a dedicated smart metering infrastructure (Figure 1).

Photovoltaic Array: the solar generation unit is composed of three Jinko Solar JKM460N-54HL4R-V high-efficiency modules (Jinko Solar Co., Ltd., Shanghai, China). Each panel has a rated peak power of 460 Wp, resulting in a total installed capacity of 1.38 kWp [19]. To minimize wiring losses and ensure optimal voltage levels for the inverter, the modules are connected in series.

The array is mounted on the balcony railing with a fixed tilt angle of 60° and an azimuth 35° west of due south (i.e., not exactly south-facing), strategically chosen to maximize solar yield during the winter months when the sun path is lower and the region often experiences diffused light conditions. The 60° tilt is also the lowest inclination at which the modules can be installed on the balcony without protruding excessively from the façade (Section 3.1). The installation was carried out in full compliance with local building regulations, ensuring both the structural safety of the railing mounts and adherence to urban landscape constraints, which are essential requirements for the sustainable integration of photovoltaics in residential areas.



Figure 1. Photograph of the experimental site, showing the three 60°-tilted photovoltaic modules, oriented 35° west of due south, mounted on the balcony railing, as described in Section 2.1.

Inverter and Power Management: power conversion and overall energy routing are managed by an Anern ECO-6200 hybrid inverter (Guangzhou Anern Energy Technology Co., Ltd., Guangzhou, China). This 6 kW unit was configured in a strict "zero feed-in" mode. This setting actively prevents any surplus generation from being exported to the public grid, making the system highly dependent on self-consumption and energy storage to prevent power curtailment. This inverter class was selected because, at the time of the experiment, the small-scale hybrid inverter market offered no intermediate option between microinverters—which cannot manage battery storage or enforce a zero feed-in constraint—and off-grid-capable hybrid inverters, which are manufactured almost exclusively in large power classes designed for whole-house backup; a 6 kW unit was therefore the smallest commercially available hybrid inverter meeting the zero feed-in and battery-integration requirements of the study, despite being oversized relative to the balcony system's own 1.38 kWp array and the simulated load. The PV array supplies the household loads directly through the inverter and charges the battery; the battery discharges to the loads when PV generation is insufficient; and the grid supplies the loads whenever PV generation and battery discharge are insufficient, as well as the inverter's own standby consumption. The grid never recharges the battery (Figure 2), as confirmed operationally by the BMS entering its low state-of-charge (SOC) protection (freeze) state at the end of low-production days.

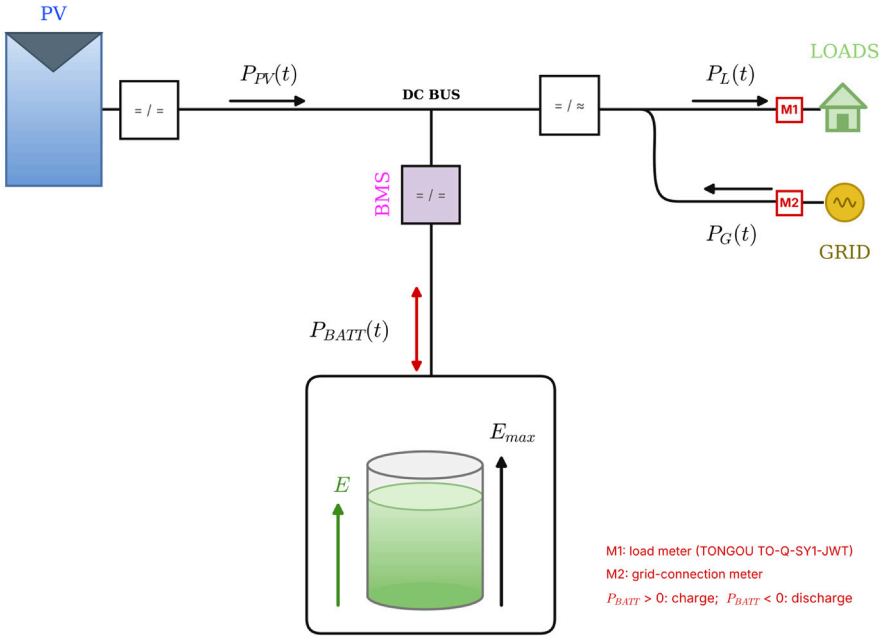


Figure 2. Block diagram of the system's power-flow architecture. PV power $P_{PV}(t)$ enters the DC bus through an MPPT DC/DC stage; a DC/AC inverter stage routes power to the household loads $P_L(t)$. In this implementation the zero feed-in configuration restricts $P_G(t)$ to import only. A bidirectional DC/DC stage, managed by the BMS, charges and discharges the battery (state of charge $E(t)$, capacity E_{max}) from the same DC bus. The battery power $P_{BATT}(t)$ is bidirectional (positive when charging, negative when discharging). M1 and M2 mark the two smart energy meters (TONGOU TO-Q-SY1-JWT, Class 1.0): M1 on the load line (AC side, load energy), M2 at the grid connection point (grid import).

Battery Energy Storage System (*BESS*): to enable load shifting—specifically transferring solar energy harvested during the day to cover the evening demand peak—the system is equipped with an Oasesenergy 51 V, 50 Ah Lithium Iron Phosphate ($LiFePO_4$) battery (Oasesenergy, China). This provides a nominal energy storage capacity of approximately 2.56 kWh. The battery pack includes a built-in Battery Management System (BMS) to ensure safe operation, prevent deep discharges, and optimize the charge/discharge cycles. The BMS is configured with a minimum SOC of 20%, so that the maximum depth of discharge (DoD) per cycle is 80% and the usable energy per cycle is 2.048 kWh. The implications of this depth of discharge for battery lifetime and for the financial analysis are discussed in Section 3.9. The BMS stops the discharge below the configured minimum SOC and stops the charge at temperatures below 0 °C. The battery was housed in a weatherproof enclosure mounted on the balcony itself, shielded from direct rain and humidity but thermally exposed to the external ambient conditions reported in Table 1, a factor relevant to the temperature-dependent $LiFePO_4$ aging discussed in Section 3.9.

Table 2 summarizes the key electrical parameters of the PV source, inverter, and BESS.

Monitoring and Data Acquisition: to accurately track the system's energy flows and calculate key performance indicators, the setup incorporates two TONGOU TO-Q-SY1-JWT (Changyou Technology (Zhejiang) Co., Ltd., Yueqing, China) smart circuit breakers equipped with integrated energy metering functions, rated to a Class 1.0 energy measurement accuracy. The first smart meter is installed on the load line to continuously log the total energy consumption of the simulated domestic profile. The second meter is positioned at the grid connection point to exclusively measure the supplementary energy drawn from the national grid. Data regarding PV generation and battery SOC were continuously acquired through the inverter's internal telemetry. The load meter and the grid meter measure on

the AC side of the system (the load line downstream of the inverter output, and the grid connection point, respectively), whereas PV generation is taken from the inverter telemetry on the DC (PV-input) side, upstream of the inverter; Equation (2) therefore accounts for all conversion, battery and standby losses between these boundaries. Since the battery is charged exclusively from the PV array, the grid import is entirely accounted for by the load and the inverter's own standby consumption. Solar irradiance was measured by two instruments. A Vevor YT60234 weather station (Fujian Youtong Industries Co., Ltd., Fuzhou, China), whose outdoor unit records the global horizontal irradiance (GHI) with a horizontally mounted radiation sensor, logged at 10 min intervals, provided the GHI record used to compute DPSH and MPSH (Section 2.2); its radiation sensor is a silicon sensor (Fine Offset WH65 chipset) with a resolution of 1 W/m^2 and an accuracy of ±15%; being a low-cost weather-station sensor rather than a calibrated reference pyranometer, it limits the accuracy of DPSH, MPSH and of the quantities derived from them (Section 3.3). A Fluke FLK-IRR2-BT irradiance meter (Fluke Corporation, Everett, WA, USA; declared measuring range 50–1400 W/m^2, resolution 1 W/m^2, accuracy ±(5% + 5 digits)), the "module plane sensor" in the following, was mounted on the plane of the modules, i.e., on the 60° tilted plane, and provided the module-plane peak irradiance values reported in Section 3.1. No transposition model was applied: the horizontal GHI is used as measured, as the reference for the theoretical yield, whereas the module-plane values are direct measurements.

Table 2. Electrical parameters of the photovoltaic source, inverter, and battery energy storage system. * Maximum charge voltage as configured in the battery's BMS.

Parameter	Value
PV string (3 modules in series, STC)	
Open-circuit voltage, Voc	120.51 V
Short-circuit current, Isc	14.14 A
Voltage at maximum power, Vmp	100.80 V
Current at maximum power, Imp	13.69 A
Inverter (Anern ECO-6200)	
MPPT voltage range	60–450 Vdc
Rated AC output power	6200 W
Battery (Oasesenergy LiFePO$_4$, 16S)	
Nominal voltage	51.2 V
Maximum voltage (BMS-configured) *	58.4 V

2.2. Load Profile and Data Acquisition

To replicate a realistic residential scenario, a daily domestic consumption profile was programmed and applied to the system, corresponding to an average of approximately 6 kWh per day over the monitoring year (2309 kWh in total, i.e., 6.3 kWh/day); this is an annual average, since a climate-control load is added in the warmer and in the spring months (Table 3). The simulated load profile consists of a continuous, fluctuating baseload ranging from approximately 50 W to 150 W, specifically designed to mimic the intermittent operation of a domestic refrigerator compressor alongside the standby power consumption of typical household appliances.

Superimposed on this continuous baseload are three distinct high-power demand periods, with programmed peak loads reaching approximately 1.1 to 1.15 kW. As depicted by the programmed load curve, these peaks are scheduled as follows:

Morning peak: Occurring between 07:00 and 08:00, simulating early morning domestic activities.

Table 3. Monthly performance summary over the 365-day monitoring period (8 May 2025–7 May 2026). * Partial calendar months at the edges of the 365-day monitoring window (8–31 May 2025: 24 days; 1–7 May 2026: 7 days). EAI values are computed on the monthly aggregated net energy benefit and system losses (Equation (4)); the annual value refers to the whole 365-day window. Column key: E_{load}, E_{PV} and E_{grid} are the monthly household energy demand, photovoltaic generation and grid draw (kWh), respectively; DPSH and DMSH are the Daily (theoretical and actual) Peak/Metered Sun Hours, i.e., the Monthly Peak Sun Hours (MPSH) and Monthly Metered Sun Hours (MMSH) each averaged per day in that month (Section 3.3); MMSH/MPSH is their ratio, equal to the monthly PV Performance Ratio (PV-PR); SSR is the Self-Sufficiency Ratio (Section 3.2); EAI is the Energy Advantage Index (Section 3.6).

Month	E_{load} (kWh)	E_{PV} (kWh)	E_{grid} (kWh)	DPSH (h)	DMSH (h)	MMSH/MPSH (%)	SSR (%)	EAI	Savings (€)
May 2025 *	138.1	130.4	59.6	5.64	3.94	69.9	56.8	1.51	23.5
June 2025	208.9	202.6	80.0	6.32	4.89	77.4	61.7	1.75	38.7
July 2025	221.5	205.3	97.1	5.76	4.80	83.4	56.2	1.54	37.3
August 2025	222.1	170.4	110.5	4.88	3.98	81.6	50.3	1.90	33.5
September 2025	216.6	133.3	135.5	3.87	3.22	83.2	37.5	1.56	24.3
October 2025	218.5	95.6	176.7	2.54	2.23	88.1	19.2	0.78	12.6
November 2025	137.1	57.9	138.9	1.46	1.40	96.1	−1.3	−0.03	−0.5
December 2025	142.5	34.1	170.7	0.86	0.80	92.7	−19.8	−0.45	−8.4
January 2026	150.5	39.2	176.4	0.96	0.92	95.9	−17.2	−0.40	−7.8
February 2026	161.2	69.0	145.2	1.99	1.79	89.8	9.9	0.30	4.8
March 2026	204.4	123.9	136.1	3.15	2.90	91.9	33.4	1.23	20.5
April 2026	229.4	175.5	106.2	4.70	4.24	90.2	53.7	2.35	36.9
May 2026 *	58.1	39.9	29.4	5.16	4.13	80.0	49.4	2.56	8.6
Annual total	2309.0	1477.1	1562.4	—	—	83.6	32.3	1.02	224.0

Afternoon peak: An extended high-demand period lasting approximately three hours (roughly 12:15 to 15:15), representing a programmed daytime appliance usage (e.g., cooking, washing).

Evening peak: Occurring from approximately 18:15 to 20:00, coinciding with evening household routines.

The load was generated with real appliances driven by programmable smart plugs, following the schedule above. Among them, an air conditioner (peak power ≈ 900 W) was the sole cooling source of the monitored apartment and was switched on automatically whenever the indoor temperature exceeded 27 °C. In winter, space heating was provided by a gas-fired radiator system independent of the monitored electrical system, and therefore not included in the recorded load; since the radiators were on, the heating mode of the air conditioner (setpoint 19 °C) never started in winter. In spring (from March onwards), once the radiators were switched off in compliance with the municipal regulation, the air conditioner operated in heating mode to keep the apartment above 19 °C. The "1.1–1.15 kW" quoted above therefore refers only to the three programmed base peaks: during the warm months the air-conditioning load adds to them (e.g., the ≈1.9 kW evening peak of a summer day, Section 3.3). Together with the spring heating use, this explains the seasonal variation in the monthly load energy in Table 3, from ≈4.6 kWh/day in November–January to ≈7.0–7.2 kWh/day in June–October and up to ≈7.6 kWh/day in April 2026.

This scheduling was a deliberate methodological choice rather than an attempt to reproduce a statistically average, unmanaged Italian household. The afternoon peak in particular was positioned to overlap with the system's highest-irradiance hours, consistent with the behaviour of an informed, load-aware prosumer who consciously times discretionary consumption (e.g., programming major appliances around midday rather than in the evening) to align with local PV generation. This choice isolates the technical and economic potential of the PV-BESS system under favourable, but realistically achievable, user

conduct; the Self-Sufficiency Ratio and economic indicators reported in Section 3 should accordingly be interpreted as characterizing this load-matching operating mode, rather than as an average expectation for a passive, unmanaged household load. The measured annual SSR of 32.3% (Section 3.2) is closely tied to the programmed, near-perfect overlap between the afternoon load block and the solar generation peak, and a real household's consumption is inevitably more stochastic than a fixed, repeating schedule. The profile does not represent the habits of one specific occupant: it depicts the archetype of an informed prosumer, so that the results indicate what is achievable by any balcony-PV owner willing to adapt their consumption timing.

The profile is a synthetic schedule designed on engineering grounds, not derived from a published empirical load-monitoring methodology: the three peaks were deliberately programmed to occur under three distinct operating conditions of the system (an early-morning peak, with the battery depleted and PV production low; a midday peak, with the battery partially charged and PV production high; and an evening peak, with the battery at its maximum daily charge and no PV production). The same schedule was repeated every day of the monitoring year, without distinguishing weekdays from weekends and public holidays, and its baseload and programmed peaks were not modified with the seasons; the seasonal variation in the recorded load (Table 3) results only from the thermostat-controlled air-conditioning load described above, superimposed on the programmed profile (cooling above an indoor temperature of 27 °C and, once the radiators were off, heating below 19 °C). Real consumption instead varies from day to day, between working days and weekends or holidays, and across seasons, so that transferring the results to other households would require the same analysis with measured or standardized load profiles, which is left to future work.

The block diagram illustrating the energy flows exchanged between photovoltaic modules, the inverter, the battery, the grid, and household loads is shown in Figure 2.

The complete daily load profile, alongside a representative daily PV generation curve, is illustrated in Figure 3. The system's performance was monitored continuously over a 365-day period. To comprehensively evaluate the system's efficiency and grid independence, four primary parameters were logged daily: the total energy consumed by the simulated load, the PV energy generated and directly utilized by the system (including battery charging), the supplementary energy drawn from the power grid, and the global solar irradiance, continuously recorded by a dedicated on-site weather station via the horizontal GHI sensor of the Vevor YT60234 weather station (as distinct from the module plane sensor of Section 2.1). The complete 365-day daily dataset for all four logged quantities is provided as Supplementary Materials to support independent verification and reuse. In addition to the instantaneous daily peak irradiance value reported for descriptive purposes in Section 3.1, this 10 min irradiance record was numerically integrated over each day and summed over each calendar month to obtain the theoretical Monthly Peak Sun Hours (MPSH)—the equivalent number of hours of standard 1000 W/m^2 irradiance that month's total insolation represents—which is used as the clipping-free reference yield in the curtailment analysis of Section 3.3; dividing by the number of days in the month gives the Daily Peak Sun Hours (DPSH) reported in Table 3. The same monthly PV yield was analogously expressed in these equivalent-hours units as the Monthly Metered Sun Hours (MMSH), computed as the ratio between that month's metered PV energy output and the array's rated peak power (1.38 kWp), with the corresponding daily average given by the Daily Metered Sun Hours (DMSH); the ratio MMSH/MPSH (=DMSH/DPSH, Section 3.3) thus represents the fraction of the theoretical solar resource actually captured by the system, defining the PV Performance Ratio (PV-PR, Section 3.3).

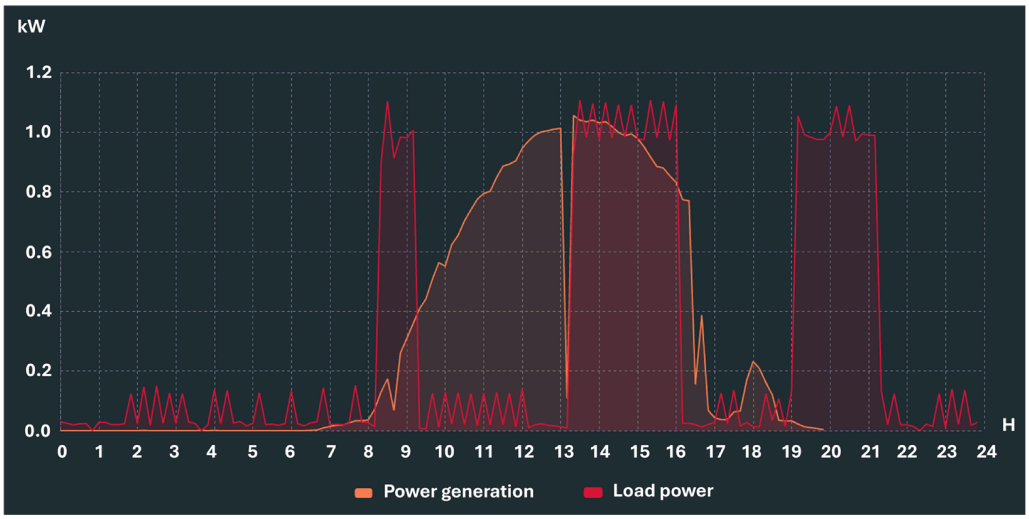


Figure 3. Example of daily consumption and PV generation profiles of the analysed system (i.e., 31 March 2026).

3. Results and Discussion

Table 3 summarizes, on a monthly basis, the key generation, consumption, self-sufficiency and economic quantities discussed throughout this section, and is referenced from Sections 3.1–3.4, 3.6 and 3.7.

3.1. Seasonal Energy Yield and the Impact of a 60° Tilt Angle

The generation profile of the balcony-mounted PV system was closely monitored over the 365-day period, revealing significant seasonal variations. These fluctuations were heavily influenced by the specific climatic conditions of the Po Valley (Emilia-Romagna, Italy) and the deliberate design choice of a 60° tilt angle for the module array, which is the lowest inclination at which the modules can be installed on the balcony: flatter angles would make the panels protrude excessively from the façade, in conflict with architectural decorum and with the right of view of neighbouring dwellings, and therefore do not allow the 30–35° recommended at this latitude for roof- or ground-mounted systems. Over the entire monitoring year, the system generated a total of 1477 kWh of photovoltaic energy. This corresponds to a specific yield of 1070 kWh/kWp for the 1.38 kWp array; including the unrealized energy discussed in Section 3.3, the total production potential of the system is about 1766 kWh, i.e., a specific yield of 1280 kWh/kWp per year—94.0% of the 1361 kWh/kWp theoretical annual yield that PVGIS [20] estimates for a fixed array at this latitude with the same 35°-west-of-south azimuth and 60° tilt, an independent cross-check that corroborates the weather-station-derived MPSH values used throughout this study. The influence of the inclination of balcony-integrated solar panels, from 0° to 90°, on the monthly and annual electricity consumption of a residential building has recently been investigated by simulation [12]; the present measurements provide a field counterpart for a steep (60°) inclination.

During the winter months (December to February), the steep 60° inclination is able to optimize the angle of incidence of solar radiation, partially compensating for the lower solar altitude. The experimental data confirms that on clear-sky winter days, the maximum daily irradiance reached peaks of 780 W/m^2 (measured by the module plane sensor), allowing the system to achieve a daily energy yield of up to 4.84 kWh. However, the overall winter performance was severely constrained by the macro-climatic characteristics of the region, which is prone to prolonged periods of dense fog and heavy cloud cover. Consequently, the

average daily PV yield during winter plummeted to 1.58 kWh, resulting in a heavy reliance on the grid to meet the simulated 6 kWh daily load.

Conversely, the system's behaviour during the summer months (June to August) highlighted the specific dynamics of a zero feed-in configuration. While a standard tilt angle of 30° to 35° is typically recommended for maximizing annual yield at this latitude [20], the balcony 60° tilt effectively flattened the midday generation curve. The maximum daily irradiance recorded during summer was 990 W/m^2—measured by the module plane sensor—yielding an average daily production of 6.29 kWh.

From an energy management perspective, this sub-optimal summer angle proved to be highly beneficial for a zero feed-in setup. By flattening the generation peak, the 60° tilt reduced the instantaneous power excess during the central hours of the day. This geometric curtailment organically mitigated the system's active clipping effect, preventing the 6 kW hybrid inverter from aggressively throttling down production when the 2.56 kWh BESS reached full capacity and the domestic load was at its baseload level. The energy yield was therefore spread more evenly throughout the daylight hours, allowing for a more efficient utilization of the available storage capacity.

3.2. Self-Sufficiency Ratio (SSR) and Battery Performance

To comprehensively evaluate the system's ability to operate independently from the public grid, the Self-Sufficiency Ratio (SSR) was calculated on a daily basis. The SSR represents the percentage of the simulated domestic load that is covered by the local PV-BESS system rather than the grid, and is defined by the following equation:

$$\mathrm{SSR} = \frac{E_{\mathrm{load}} - E_{\mathrm{grid}}}{E_{\mathrm{load}}} \times 100\% \quad (1)$$

where E_{load} is the total daily energy demand (mainly maintained at approximately 6.33 ± 1.34 kWh), E_{grid} is the supplementary energy drawn from the utility network, and E_{PV} is the PV energy actually utilized by the system, either instantaneously or after storage in the battery. Over the 365-day monitoring period, the system achieved an average annual SSR of 32.34%. It is worth noting that this figure is substantially lower than the nominal ratio between annual PV generation and annual load ($E_{\mathrm{PV}}/E_{\mathrm{load}} = 1477.1/2308.96 = 63.97\%$), i.e., the fraction of consumption that the year's PV output would cover if perfectly time-matched. The difference is entirely attributable to the system losses L, defined as the part of the energy entering the system (PV generation plus grid intake) that does not reach the load:

$$L = (E_{\mathrm{PV}} + E_{\mathrm{grid}}) - E_{\mathrm{load}} - \Delta E_{batt} \quad (2)$$

where ΔE_{batt} is the net change of the energy stored in the battery between the start and the end of that period. In the present system this term is negligible on the daily time scale: the evening peak (18:15–20:00) was programmed to draw approximately 2 kWh or more, comparable to the usable capacity of the battery (2.048 kWh, Section 2.1), and, with no grid charging, the battery therefore starts each day at, and returns by the end of each day to, the same minimum SOC threshold, so that $\Delta E_{batt} \approx 0$ between consecutive days. Moreover, since the stored energy is bounded by this usable capacity, ΔE_{batt} over any aggregation window can never exceed 2.048 kWh, i.e., 0.07% of the 3039.4 kWh entering the system over the monitoring year and 0.28% of the annual losses (730.5 kWh), so that the daily, monthly and annual values of L and of the EAI are not materially affected. The SOC series logged by the inverter is not part of the released dataset and was not reprocessed; the end-of-day condition therefore rests on the design and operation of the system.

Thus neglecting ΔE_{batt}, since $E_{\text{load}} - E_{\text{grid}} = E_{\text{PV}} - L$ by construction, the SSR can be rewritten as:

$$\text{SSR} = \frac{E_{\text{PV}} - L}{E_{\text{load}}} \times 100\% \quad (3)$$

With the annual values ($L = 730.5$ kWh, i.e., 24.03% of the 3039.4 kWh entering the system), this gives 63.97% − 31.63% = 32.34%: the gap between nominal coverage and realized self-sufficiency is fully accounted for by the system losses. No separate temporal-mismatch penalty needs to be invoked to explain this shortfall; that mismatch is instead the direct cause of the clipping (Section 3.3) and of the winter Appliance Paradox (Section 3.5) discussed below. It is worth noting that the SSR is not directly comparable to the self-consumption rate cited in Section 1 for storage-less systems, since the two ratios have different denominators (household load vs. PV production); expressed on that same production basis, the present system's self-consumption rate is $(E_{\text{load}} - E_{\text{grid}})/E_{\text{PV}} = 50.5\%$, modestly exceeding the 45% benchmark for storage-less systems, consistent with the expected benefit of battery integration. This metric, however, exhibited profound seasonal fluctuations. During the summer months, the integration of the $LiFePO_4$ battery allowed the system to reach a peak seasonal SSR of 55.8%, with the single best day reaching 84.7% self-sufficiency. Conversely, the winter SSR turned negative, averaging −10.6%, directly reflecting the reduced solar yield and the high frequency of overcast days typical of the geographical location. The experimental data unequivocally demonstrates that the BESS was the critical component in maximizing self-sufficiency. In standard plug-and-play balcony systems without storage, the SSR is strictly limited to the instantaneous intersection of the PV generation curve and the daytime load profile. In the tested configuration, the battery consistently absorbed the surplus solar generation during the afternoon period (12:15 to 15:15), when the continuous baseload was low and generation was high. Most importantly, the BESS successfully performed daily load shifting, discharging to cover the evening demand peak (18:15 to 20:00). Data shows that on optimal solar days, the usable capacity of 2.048 kWh was sufficient to completely power the evening peak almost without grid intervention, depleting the battery to the BMS minimum SOC just as the high-demand period concluded. This shifting capability validates the necessity of storage integration to overcome the inherent limitations of pure self-consumption in multi-dwelling residential environments.

3.3. The Curtailment Phenomenon ("Clipping" Effect)

A primary objective of this experimental setup was to quantify the energy curtailment, commonly referred to as the "clipping effect," which is inherent to zero feed-in configurations. In regions with high solar potential during the summer, the regulatory or technical prohibition of grid export creates a significant bottleneck for system efficiency. Throughout the monitoring period, particularly during high-irradiance spring and summer days, the $LiFePO_4$ battery frequently reached a 100% State of Charge (SOC) by early afternoon. Once the storage capacity was saturated and the simulated domestic load reverted to its minimal baseload state (fluctuating between 50 W and 150 W), the hybrid inverter actively intervened. To maintain the zero feed-in constraint, the inverter curtailed the power output of the 1.38 kWp PV array to perfectly match the instantaneous domestic demand.

Consequently, the experimental data reveals a substantial disparity between the theoretical solar yield and the actual energy harvested. It is estimated that during the peak solar months, an average of 1.50 kWh per day of potential renewable energy was curtailed. Over the entire 365-day period, this resulted in a total unrealized energy yield of approximately 289.1 kWh. Expressed as specific yield, the 1070.3 kWh/kWp actually utilized and the 209.5 kWh/kWp unrealized add up to a total production potential of 1279.8 kWh/kWp per year (1766.2 kWh for the 1.38 kWp array), of which 83.6% was utilized.

This phenomenon visually manifested in the daily generation curves as a sudden, flat plateau or a drastic drop in PV power matching the baseload, occurring precisely when irradiance was at its highest (Figure 4). The extent of this clipping effect highlights a structural limitation of pure zero feed-in setups for balcony applications. It demonstrates that without mechanisms to export surplus power to the grid, a significant portion of clean energy is inevitably wasted, suggesting the need for either larger, potentially less cost-effective local storage, or updated regulatory frameworks that allow and valorize micro-scale energy exchange from multi-dwelling buildings.

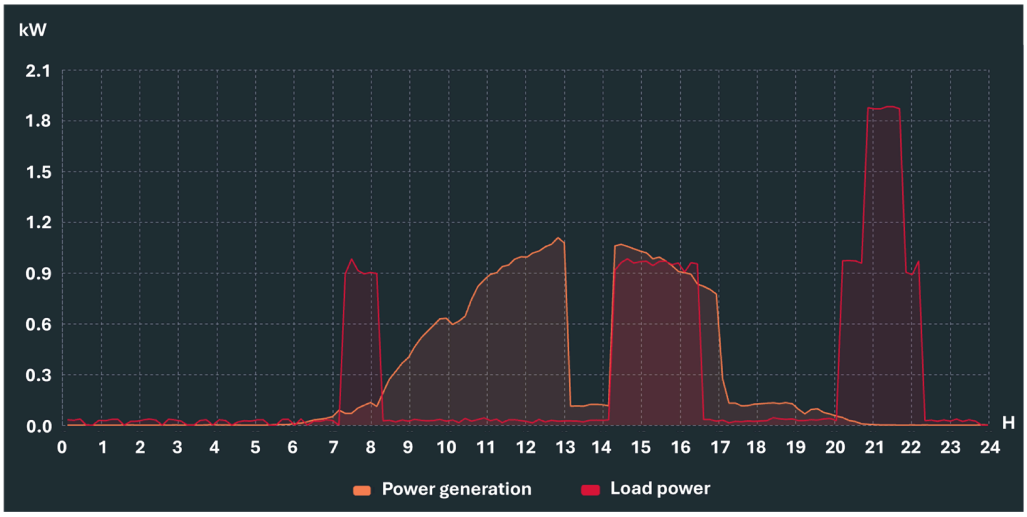


Figure 4. Daily profile of photovoltaic generation and consumption, clearly showing the phenomenon of generation curtailment between 1 p.m. and 2 p.m., and after 5 p.m.

The ratio between actual (MMSH) and theoretical (MPSH) solar yield defines what we term the PV Performance Ratio (PV-PR), equal to 83.6% on an annual basis. The PV-PR is computed at the PV array stage only: its numerator is the PV energy metered by the inverter telemetry (after zero feed-in curtailment) and its denominator the energy obtainable from the measured solar resource without curtailment, so that it reflects the capture losses upstream of the inverter (e.g., thermal, wiring and mismatch losses) and the zero feed-in clipping, but not the inverter, battery and cabling losses that enter the end-to-end Performance Ratio of IEC 61724, which is not computed in this study. Moreover, since the reference irradiance is measured on the horizontal plane, the PV-PR also incorporates the effect of the 60° tilt and the orientation of the array. Furthermore, the accuracy of the irradiance sensor (±15%, Section 2.1) propagates proportionally to MPSH, to the unrealized energy and to the PV-PR. The comparison with the PR values reported for grid-connected systems without storage is therefore indicative only; for these systems, the European PV Guidelines consider 80–85% a good result and values below 75% indicative of a fault [21]. Despite the aggressive 60° tilt angle and the zero feed-in clipping constraint, the system's PV-PR sits at the upper end of this range. This favourable figure should not, however, be confused with the markedly lower PR values reported for off-grid systems in which storage and distribution losses are included within the same metric: a recent case study of an off-grid PV mini-grid in rural Ethiopia reported a temperature-corrected PR of only 42% once battery and distribution losses were accounted for [22]. The comparison indicates that most of the shortfall between the system's high capture-stage PV-PR and its considerably lower overall SSR (32.34%, Section 3.2) originates downstream of the array—in inverter conversion, battery round-trip and standby losses—rather than in the panels' ability to capture the available solar resource. To visually summarize the overall annual energy

balance—from the theoretical solar potential down to the useful domestic load, accounting for both the curtailment effect and the downstream system losses—the complete energy flow is illustrated in the Sankey diagram in Figure 5.

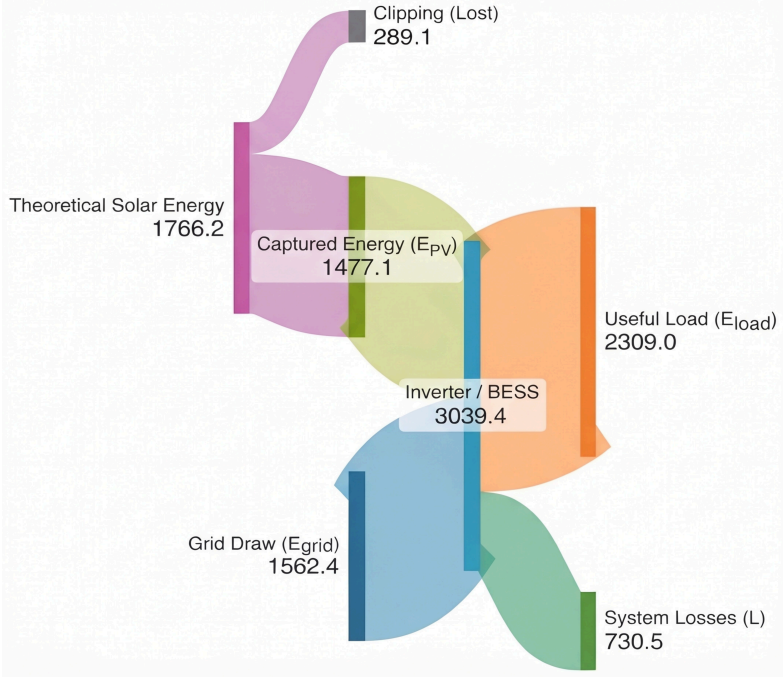


Figure 5. Sankey diagram of the annual energy flows (expressed in kWh) for the monitored PV-BESS system. The chart illustrates the transition from theoretical solar yield to actual captured energy (accounting for zero feed-in clipping), and the subsequent energy routing through the hybrid inverter and battery system, visually quantifying the net system losses (L) relative to the useful household load.

3.4. Economic Performance: Annual Savings and Summer Peaks

The ultimate feasibility of the proposed balcony-mounted PV-BESS system depends on its economic performance, specifically the capacity to generate sufficient financial savings to offset the initial Capital Expenditure (CAPEX). The system's CAPEX, encompassing the three 460 Wp modules, the 6 kW hybrid inverter, the 2.56 kWh $LiFePO_4$ battery, smart meters, and mounting hardware, totaled approximately €1100. Table 4 breaks down this total by system component.

Table 4. Capital expenditure (CAPEX) breakdown by system component.

Component	Cost (€)
Solar modules	200
Inverter	300
Battery	400
Wiring	20
Smart monitoring	30
Mounting brackets	150
Total CAPEX	**1100**

The economic viability of the balcony-mounted PV-BESS system is primarily evaluated through the direct financial savings generated by avoided grid energy purchases. Over the full 365-day experimental campaign, the system produced a total net saving of 224 €. This figure accounts for the entirety of the solar energy successfully harvested and utilized

by the household load, valued at the average national electricity tariff for the period of 0.30 €/kWh [23].

The system's economic productivity reached its maximum during the summer season (June to August). In this period, the combination of high solar altitude and the effective use of the 2.56 kWh $LiFePO_4$ battery for evening load shifting allowed the system to achieve its peak financial performance. Monthly savings during August reached 33.50 €, representing a reduction of approximately 50.3% in the monthly energy expenditure compared to a non-PV scenario.

When distributed across the year, the average daily saving demonstrates the system's potential as a hedge against energy price volatility, particularly during the high-irradiance months. However, the total annual return is significantly tempered by the operational challenges of the winter season (further analysed in Section 3.5), which extend the simple payback period to an estimated 4.91 years based on the CAPEX of the hardware components.

3.5. The "Appliance Paradox" and Seasonal System Deactivation

An unexpected and highly relevant finding of the 365-day monitoring campaign emerged during the deep winter months (specifically November, December, and January). Contrary to the standard assumption that a PV system will, at worst, provide negligible savings during periods of low irradiance, the experimental data revealed a net negative energy balance. During this quarter, the household actually consumed more energy from the grid than it would have if the PV-BESS infrastructure had not been installed. This phenomenon is defined in this study as the "Appliance Paradox."

The root cause of this paradox lies in the continuous parasitic power draw (standby consumption) of the 6 kW hybrid inverter. To power its internal electronics, maintain the Battery Management System (BMS), and sustain grid-synchronization capabilities, the inverter requires a constant background load. During the highly overcast, foggy, and short winter days typical of the Po Valley, the daily photovoltaic generation frequently failed to surpass this continuous parasitic consumption. Consequently, rather than functioning as an energy generator, the inverter effectively acted as an additional, continuous household appliance, drawing energy from the public utility to sustain its own operation.

Quantitative analysis of the dataset confirms that keeping the system active during these three months resulted in an excess grid consumption of 56 kWh compared to the baseline 6 kWh/day simulated load. This translates to a direct net financial loss of 16.80 € for the user during the winter period—equal to 42.7% of the €39.36 market value of the 131.2 kWh of PV energy the system did generate over the same three months, underscoring how severely the parasitic standby draw erodes the economic return in this season.

To address this inefficiency, an alternative operational scenario was modelled: a complete "winter switch-off." The calculations demonstrate that completely powering down the inverter and disconnecting the BESS from the grid from November to January would entirely eliminate this parasitic draw. By treating the system as a seasonal asset rather than a year-round appliance, the overall annual Return on Investment (ROI) is mathematically improved.

This counter-intuitive operational strategy highlights a critical vulnerability in the deployment of high-capacity hybrid inverters for small-scale balcony systems in low-irradiance climates. It demonstrates that the mismatch between the inverter's standby power and the minimal winter PV yield necessitates a paradigm shift in system management, suggesting that seasonal deactivation may be a mandatory practice to optimize the economic viability of multi-dwelling residential microgrids.

3.6. The Energy Advantage Index (EAI) and Predictive Seasonal Deactivation

To systematically determine the optimal operational window and mitigate the "Appliance Paradox" observed during the winter months, a novel metric defined as the Energy Advantage Index (EAI) is introduced. The EAI quantifies the dynamic relationship between the net energy benefit provided to the household and the inherent operational losses of the system architecture. The net energy benefit is calculated as the difference between the total domestic energy demand and the supplementary energy drawn from the grid ($E_{\text{load}} - E_{\text{grid}}$). The system losses L are those defined by Equation (2) (with ΔE_{batt} negligible, as discussed in Section 3.2), i.e., the difference between the total energy entering the system (photovoltaic generation plus grid intake) and the energy effectively utilized by the load. The EAI is therefore formulated as follows:

$$\text{EAI} = \frac{E_{\text{load}} - E_{\text{grid}}}{\left(E_{\text{PV}} + E_{\text{grid}}\right) - E_{\text{load}}} = \frac{E_{\text{load}} - E_{\text{grid}}}{L} \tag{4}$$

The resulting scalar value provides a direct assessment of the system's operational efficiency on a daily basis:

EAI > 1: The energy advantage strictly exceeds the system losses. The PV-BESS is operating efficiently, significantly reducing grid reliance.

$0 <$ EAI < 1: The system maintains a positive net energy balance ($E_{\text{load}} > E_{\text{grid}}$), but the internal conversion and standby losses surpass the net advantage. The system is beneficial but operating at low overall efficiency, in a loss-dominated regime; EAI $= 1$ marks the boundary with the benefit-dominated regime above.

EAI < 0: The system is in a state of net deficit. The grid is supplying more energy than the baseline domestic load requires, strictly to keep the inverter and BESS active. This mathematical threshold identifies the precise onset of the Appliance Paradox.

The intermediate range $0 <$ EAI < 1 identifies a transitional operating regime, whose meaning becomes explicit by noting that, by the definition of the system losses in Equation (2), the net energy benefit equals the PV energy minus the system losses, $E_{\text{load}} - E_{\text{grid}} = E_{\text{PV}} - L$. The index can therefore be rewritten as:

$$\text{EAI} = \frac{E_{\text{PV}} - L}{L} = \frac{E_{\text{PV}}}{L} - 1 \tag{5}$$

Within this reading, EAI $= 0$ corresponds to a PV yield exactly equal to the system losses, EAI $= 1$ to a yield equal to twice the losses, and $0 <$ EAI < 1 to a yield that covers the losses without doubling them, so that less than half of the PV energy is converted into avoided grid consumption (the converted fraction being EAI/(1 + EAI)). In this range the system still saves grid energy and money, and switching it off would forfeit a positive, if modest, saving: the criterion for seasonal deactivation is therefore EAI < 0, and not EAI < 1. Because the system losses vary comparatively little through the year (about 1.7–2.6 kWh/day as monthly averages), the position of the index is governed mainly by the PV yield: its entry into the 0–1 band from above can be read as an early warning of the approaching Appliance Paradox, while the return of the expected index above zero marks the point at which reactivation becomes worthwhile.

In the monitored year, 69 of the 365 days (19%) fell within this band. On these days the average avoided grid consumption was 0.76 kWh/day, for a cumulative saving of about €16, equal to 7% of the annual total. Most of them (45 of 69) occurred in the shoulder months, September–November and February–March, the rest being isolated days of low PV yield in the productive season and comparatively favourable days in December–January. Computed on monthly aggregated energies (Table 3), October (EAI = 0.78) and February (EAI = 0.30) fall within the band, immediately before and after the negative winter window of Section 3.5. Aggregated over the whole year, the index equals 1.02: the system operates

almost exactly at the boundary between the loss-dominated and benefit-dominated regimes, with 50.5% of the PV energy converted into avoided grid consumption.

The distribution of the EAI over the 365-day experimental campaign (Figure 6) clearly illustrates the seasonal viability of the setup. Throughout the spring, summer, and early autumn periods, the index remains robustly positive, frequently peaking at high values, albeit with significant daily fluctuations dictated by transient cloud cover and varying irradiance. However, an analysis of the winter timeline (roughly corresponding to days 300 to 365 and the initial 50 days of the year) reveals an extended, systematic collapse of the metric. During these intervals, characterized by the dense fog and low solar altitude typical of the region, the EAI drops below the zero threshold on about two thirds of the days (76 of 116) and falls within the 0–1 range on most of the remainder (34 days). On the negative days, the standby power draw of the 6 kW hybrid inverter entirely negates the scarce photovoltaic yield, dragging the system into negative efficiency. Ultimately, the EAI transcends the specific parameters of this experimental setup and serves as a scalable predictive tool. It provides a standardized method to calculate the optimal seasonal deactivation window for any residential PV-BESS configuration. By evaluating a system's theoretical parasitic losses against estimated localized winter photovoltaic yield, the EAI allows system designers and smart energy management platforms to pre-emptively predict when a microgrid will transition from a generating asset to a net consumer. This enables the implementation of automated seasonal shut-down strategies, effectively circumventing the Appliance Paradox and maximizing the true annual economic and energy efficiency of the installation.

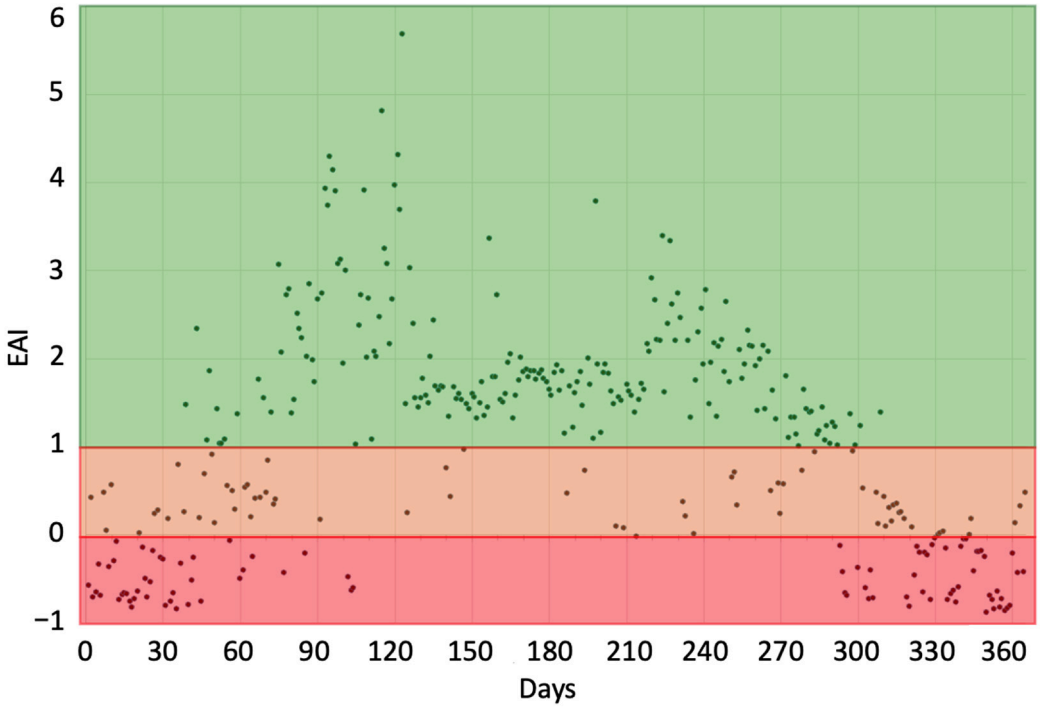


Figure 6. Daily Energy Advantage Index (EAI) over the 365-day monitoring period. For clarity, the graph is plotted against the calendar day of the year (Day 1 = 1 January; Day 300 ≈ 27 October; Day 50 ≈ 19 February) rather than against the chronological monitoring day, and therefore differing from the 8 May 2025–7 May 2026 axis used elsewhere in the paper (e.g., Table 3). Green area (EAI > 1) indicates the benefit-dominated regime; orange area (0 < EAI < 1) the loss-dominated but still favourable transitional band; red area (EAI < 0) the net-deficit regime underlying the winter Appliance Paradox.

The two energy meters are specified at Class 1.0 (±1% of reading), and no independent calibration data beyond this manufacturer declaration are available. In the worst case, in which the load and grid meters err by 1% in opposite directions, the uncertainty of the net benefit $E_{load} - E_{grid}$ is $0.01 \times (E_{load} + E_{grid})$, i.e., between ±1.4 and ±2.2 percentage points of SSR on a monthly basis and ±38.7 kWh (±1.7 percentage points, SSR = 32.3 ± 1.7%) on the annual one, which leaves the seasonal pattern unchanged (summer SSR above 50%, winter SSR negative). In November (E_{load} = 137.1 kWh, E_{grid} = 138.9 kWh, SSR = −1.3%) the net difference of −1.8 kWh is smaller than this bound (±2.8 kWh), so the sign of that month's net benefit is not resolved by the measurement, whereas those of December (−28.2 kWh) and January (−25.9 kWh) lie well outside it (bounds of 3.1 and 3.3 kWh). Since EAI < 0 is equivalent to $E_{load} - E_{grid} < 0$ (Equation (5)), the same criterion applies on a daily basis: on 8 of the 365 days the net benefit lies within the daily bound $0.01 \times (E_{load} + E_{grid})$, and of the 65 negative-EAI days of November–January, 63 lie outside it and are therefore reliably identified as negative, the remaining two being indeterminate. The uncertainty of the PV telemetry, which enters L and hence the magnitude of the EAI but not its sign, was not assessed.

3.7. Inverter Oversizing and Partial-Load Efficiency Penalties

A critical correlation observed in the monthly data matrix pertains to the overall conversion efficiency of the system architecture. The experimental setup utilizes a 6 kW hybrid inverter to manage a simulated daily load of 6 kWh, characterized by an extended baseload of merely 50 W to 150 W and absolute peak demands not exceeding 1.15 kW.

Throughout the operational year, the inverter consistently operated at a small fraction of its nominal capacity (frequently below 5%). Standard power electronics exhibit a severe degradation in conversion efficiency under extreme partial-load conditions, a behaviour formally characterized by the weighted efficiency measurement procedures of IEC 61683 [24]. The manufacturer's datasheet for the Anern ECO-6200 itself reports a peak efficiency of 93% and a no-load power consumption of 50 W [25], a figure that alone accounts for a substantial share of the parasitic standby draw quantified in Section 3.5. Independent laboratory testing of comparable hybrid inverters at very low partial loads, recently conducted by HTW Berlin in cooperation with the Austrian Institute of Technology and the Karlsruhe Institute of Technology, found conversion efficiencies at an output of only 150 W ranging from 64% to 90% depending on the model [26], confirming that the efficiency collapse observed here at a comparable operating point is consistent with published results for similar hardware. Consequently, the data reveals that the system losses are not solely attributable to the fixed parasitic standby draw (discussed in Section 3.5), but are significantly compounded by poor DC-to-AC conversion efficiencies during the extended low-demand periods. This highlights a fundamental design conflict in balcony PV-BESS systems: while high-capacity hybrid inverters are often required to support significant battery integration and handle isolated high-power appliances, their massive oversizing relative to the continuous baseload inherently throttles the net energy advantage of the microgrid.

This finding suggests a practical, prospective use for the EAI beyond the retrospective seasonal-deactivation analysis of Section 3.6: since EAI < 0 is algebraically equivalent to $E_{PV} < L$ (Equation (5)), a system designer can estimate, before installation, whether a given PV-inverter pairing is at risk of winter net-negative operation by comparing the inverter's rated losses—its no-load standby plus the partial-load conversion losses implied by its efficiency curve, not the no-load figure alone—against the worst-case or low-percentile daily PV yield expected for the site's latitude and tilt, itself obtainable from a database such as PVGIS [20] as demonstrated in Section 3.1. Applied retrospectively to the present system, a simplified screening that considers standby energy consumption only (Table 5)

gives the following result: a standby draw below approximately 10 W would have left no day of the measured 2025–26 winter (0 of 92) on which the PV yield falls below the standby energy alone, compared with 41 of 92 days (44.6%) for the installed inverter's 50 W specification. This screening is, however, a lower bound on the number of negative-EAI days, because it neglects the conversion and battery losses included in Equation (2): with the measured losses L, 65 of the 92 November–January days (70.7%) have EAI < 0 for the installed unit, the measured winter losses averaging 2.03 kWh/day against a standby energy of 1.2 kWh/day (50 W × 24 h). A low standby power is therefore a necessary, but not a sufficient, condition for avoiding the Appliance Paradox. The 10 W figure should not be read as a universal physical threshold, since it is anchored to the single coldest, foggiest day of one monitored winter and would shift with the inter-annual weather variability discussed in Section 4; rather, it illustrates that the EAI framework doubles as a sizing-validation criterion, allowing the Appliance Paradox to be anticipated and designed around—through inverter selection or a pre-planned deactivation schedule—rather than discovered only after a full season of operation.

Table 5. Simplified screening considering standby energy consumption only: sensitivity of the number of negative-EAI winter days (November–January, 92 days) to the assumed inverter standby power, computed from the measured daily PV yield of this study (this work).

Assumed Standby Power (W)	Negative-EAI Days (of 92)	Share of Winter Days (%)
10	0	0.0
15	4	4.3
30	31	33.7
50 (installed unit)	41	44.6

3.8. The "Shoulder Season" Optimum: Geometric vs. Climatic Constraints

Analysis of the monthly performance metrics reveals a distinct operational "sweet spot" during the shoulder seasons (specifically the periods encompassing March to May, and September to October). While summer typically represents the peak generation period for standard PV installations, this balcony setup is subject to a unique intersection of geometric and macro-climatic constraints.

The 60° tilt angle of the modules is geometrically optimized for low solar altitudes. However, the expected winter yield is consistently undermined by the frequent days of fog and persistent cloud cover typical of the Po Valley. Conversely, during the peak summer solstice, the high solar altitude results in a highly sub-optimal angle of incidence for the 60° array, geographically limiting the maximum generation potential (which, while beneficial for mitigating zero feed-in clipping, reduces overall hardware efficiency).

The shoulder seasons emerge as the optimal performance window. During the vernal and autumnal equinoxes, the solar altitude aligns perfectly with the 60° tilt, yielding the highest system efficiency. The monthly data reflects this alignment, showing optimal load-matching, maximized battery throughput, and the highest sustained Energy Advantage Index (EAI) prior to the onset of the severe winter climatic constraints.

3.9. Long-Term Financial Perspectives and Investment Viability

With an initial Capital Expenditure (CAPEX) of approximately €1100, the system requires an order of magnitude less upfront capital than a conventional rooftop or condominium-scale PV installation. The calculated Return on Investment (ROI) ≈ 137% significantly outperforms conventional low-risk financial instruments, such as government bonds or other low-risk investments. As a physical asset, the PV-BESS generates immediate and tangible economic value through the continuous reduction in operational utility

expenses, offering financial benefits that are difficult to replicate with standard savings vehicles over the same timeframe.

The baseline Payback Period (PBP) accounts for an assumed electricity price inflation of 3.6%/year and panel degradation (−0.3%/year). This inflation figure is a deliberately conservative assumption, corresponding to Italy's general consumer price inflation rate over 2021–2025—the geometric mean of the annual average rates reported in ISTAT's definitive year-end releases for that period (+1.9%, +8.1%, +5.7%, +1.0%, and +1.5% for 2021–2025, respectively [27])—rather than the markedly higher energy-specific inflation observed over the same period. On this basis, the PBP is inherently competitive (4.63 years); it is worth noting that the two degradation terms entering this model are not equally well characterized. The panel degradation rate is taken directly from the manufacturer's datasheet warranty curve [19] and is therefore a robust, well-documented input. The BESS capacity fade, by contrast, was not measured in this study and is not separately modelled in the payback calculation above; a cumulative capacity loss on the order of 20% over ten years is a plausible assumption for a $LiFePO_4$ cell of this type, but the actual rate depends strongly on ambient temperature, cumulative cycle count, and depth of discharge (DoD), none of which were independently tracked over the monitoring year. The BMS minimum SOC of 20% limits the DoD to 80% per cycle (Section 2.1); because the evening peak is sized to discharge the battery down to this floor, the system operates with deep daily cycles on days with sufficient PV production. Fixed-condition cycle-life tests generally indicate that deeper discharges accelerate capacity fade, whereas a comprehensive 29-month aging study on a commercial $LiFePO_4$/graphite cell found that the dependence on the cycling window is not monotonic, shallow cycling around a mid-range state of charge itself inducing an unexpectedly strong, if partly reversible, capacity loss under certain temperature conditions [28]; the net effect of the actual cycling regime on long-term capacity therefore cannot be predicted reliably from the DoD alone. As regards temperature, the battery was thermally exposed to the ambient conditions of Table 1 (monthly mean minima of 1–2 °C in December–February). Charging graphite/$LiFePO_4$ cells at low temperature can cause lithium plating and loss of cyclable lithium [29]; accordingly, the BMS stops the charge below 0 °C (Section 2.1). Sub-zero temperatures occurred on some winter days, but always in the early hours of the day, in darkness or with minimal PV production, so this cut-off is not expected to have materially restricted the charging of the battery from PV or to have affected the winter yield; this could not be verified directly, since the battery temperature was not logged. By preventing charging below 0 °C, the BMS also limits the exposure of the cells to plating conditions; the assumed 20%/10-year capacity loss nonetheless remains an assumption rather than a measured result, and should be validated with dedicated battery-health monitoring in future work. Beyond this caveat, the economic return can be further improved through active system management. Implementing targeted operational strategies—specifically, maximizing the alignment between domestic loads and solar generation to mitigate the clipping effect, and enforcing seasonal deactivation to neutralize the "Appliance Paradox"—directly enhances long-term profitability. The comparative economic matrix demonstrates that a complete system shutdown during the winter quarter, a seemingly counterintuitive measure, actually accelerates the payback period (4.33 years) and increases the projected 10-year ROI from ≈137% to ≈154% (Table 6). This targeted deactivation effectively eliminates the net financial losses incurred by the inverter's parasitic consumption during prolonged low-irradiance months.

Table 6. Main economic indicators with year-round operation and with winter switch-off (November–January).

Indicator	Year-Round Operation	Winter Switch-Off	Change
Annual saving (€)	223.98	240.75	+16.76
Simple payback period (years)	4.91	4.57	−0.34
Payback period with inflation and degradation (years)	4.63	4.33	−0.30
Ten-year ROI (%)	137	154	+17 p.p.
Electricity purchase expenditure per unit of load, CAPEX excluded (€/kWh)	0.203	0.196	−0.007

From the end-user's perspective, the most critical financial metric is the effective cost per consumed kilowatt-hour, but this is best understood in two steps. Considered in isolation, the self-generated photovoltaic energy is remarkably cheap: dividing the system's CAPEX of €1100 by its expected useful life (20 years) and its measured annual yield (1477 kWh) gives a classic, undiscounted Levelized Cost of Energy (LCOE) for the PV-BESS system of approximately €0.037/kWh—roughly 4 cents, almost an order of magnitude below the €0.30/kWh average gross cost of grid electricity in Italy. This is the intrinsic cost of the energy the system itself produces, independent of how much of it the household ultimately consumes. What determines the household's actual bill, however, is the blended cost of its total consumption, of which only the measured annual Self-Sufficiency Ratio (32.34%) is covered by this near-free self-generated energy, while the remaining 67.66% is still purchased from the grid at the full €0.30/kWh tariff. Weighting the two sources by the energy each supplies gives the effective cost per kWh actually consumed by the household: €0.215/kWh (=0.3234 × 0.037 + 0.6766 × 0.30), an approximately 28% reduction relative to the €0.30/kWh gross national average. This quantity is the cost of electricity supply per unit of load, including capital investment (via the LCOE). By contrast, the electricity purchase expenditure per unit of load, excluding capital investment (self-generated energy carrying no marginal cost, the investment being accounted for separately by payback and ROI, Table 6), is 0.30 × 67.66% = €0.203/kWh, i.e., 32% lower than the gross tariff. This blended effective-cost figure, rather than the system's own LCOE, is the metric directly relevant to the household's electricity bill, since it accounts for the share of consumption the PV-BESS system cannot cover. Once deployed, the system locks in this lower blended rate for its operational lifespan, providing a structural hedge against future grid tariff volatility.

Table 6 compares the main economic indicators of the system operated year-round with those obtained when it is deactivated during the winter quarter (November–January, 92 days), as discussed in Sections 3.5 and 3.9.

In the switch-off scenario the system produces no PV energy from November to January and the load is supplied entirely by the grid in that period. CAPEX €1100; grid tariff €0.30/kWh. Payback with inflation and degradation and ROI assume 3.6%/year electricity price inflation and −0.3%/year PV degradation. The electricity purchase expenditure per unit of load equals the grid tariff times the fraction of consumption drawn from the grid, i.e., self-generated energy carries no marginal cost, the investment being accounted for by payback and ROI; the cost of electricity supply including capital investment, obtained by weighting the LCOE (€0.037/kWh) and the grid tariff by the energy shares, is €0.215/kWh for year-round operation (Section 3.9). Changes are computed from unrounded values.

3.10. Impact on Social and Environmental Sustainability

Beyond its technical and economic performance, the balcony-mounted PV-BESS system tested in this study carries broader implications for household energy resilience and for the environmental footprint of small-scale residential electrification. This section discusses

these dimensions with reference to the same annual figures reported in Sections 3.4–3.9, extrapolated where relevant to a 10-year horizon.

3.10.1. Energy Democracy and Energy Poverty Mitigation

A defining feature of the plug-and-play PV-BESS architecture is its installation simplicity: no professional design is required, and assembly reduces to clipping the panels onto the balcony railing, connecting them to the inverter via standard MC4 connectors, and wiring the unit's output to the household's distribution board and its input to the utility meter. Current Italian regulation, however, ties the administrative burden to the inverter's rated AC output rather than to installation complexity: systems up to 350 W can be self-installed without any permit, those up to 800 W require only an electrician's declaration of conformity, and above 800 W a formal grid-connection authorization is required [30]. Because the Anern ECO-6200 used here is rated at 6.2 kW, the system falls outside this simplified regime and would strictly require formal authorization in any residential deployment—an administrative cost not reflected in the CAPEX of Table 4. However, in practice, the hardware-enforced zero feed-in configuration ensures that inverter and grid currents combine only at the load (Figure 2). This allows the system to deliver power up to its full rating without a single watt entering the grid. Consequently, its grid impact is no greater than that of a feed-in-capable sub-800 W system—a technical reality that current regulation does not yet formally recognize. This installation-level accessibility still benefits households that lack access to credit lines or accumulated savings, for whom a large one-off rooftop investment—or participation in a collective condominium project—remains out of reach, even where the connection paperwork itself is not yet simplified for zero feed-in hardware.

For the household, the practical outcome of this accessibility is a direct and recurring reduction in the electricity bill: approximately €224 in avoided grid purchases in the monitored year, rising to roughly €241 when the system is actively managed around the Appliance Paradox (Sections 3.5 and 3.6)—a reduction of up to one third of the household's electricity expenditure (SSR = 32.34%; full financial indicators are reported in Section 3.9). Because this saving displaces a fixed, unavoidable household cost rather than depending on a market-traded return, it recurs every year of the system's operational life: over a 10-year horizon it amounts to well over €2600 in cumulative avoided expenditure against an initial outlay of €1100. For a low-income household in particular, this represents a structural, compounding reduction in energy costs achieved without exposure to the collective decision-making, shared debt, or large upfront capital typically required by rooftop or condominium-scale interventions.

Taken together, these characteristics position the balcony PV-BESS system as a concrete instrument of energy democracy and a practical tool against energy poverty: a technology whose low entry cost, DIY-level installation barrier, and durable bill reduction extend the benefits of self-generation to households—including tenants and residents of social housing—who are structurally excluded from rooftop or condominium-scale solar investment, and for whom a stable, long-term reduction in electricity costs can meaningfully ease the weight of energy expenditure on household budgets.

3.10.2. Environmental Benefits

At the measured annual avoided grid consumption of 746.6 kWh, and applying the national electricity mix emission factor of 0.315 kg CO_2eq/kWh [31], the system avoids the emission of approximately 235 kg of CO_2eq per year. Projected linearly over the same 10-year horizon used for the financial analysis, and without crediting any further improvement from the seasonal deactivation strategy of Section 3.6, this amounts to approximately 2.35 tons of CO_2eq avoided per installed system.

These figures can also be expressed in more tangible terms: the same 10-year avoided emissions are equivalent to approximately 19,580 km not driven by an average Euro 6 passenger car (Italy's 2023 new-registration fleet average, 120.1 g CO_2/km) [32], or to the CO_2 sequestered over a decade by approximately 235 young urban trees (10 kg CO_2 per tree per year for a small-diameter urban specimen) [33]. Scaled hypothetically to a municipal-level deployment on the order of a thousand such systems—a scale well within reach for a medium-sized municipality, and comparable in scope to a social-housing electrification programme—these per-system figures would imply an aggregate avoidance of approximately 2350 tonnes of CO_2eq over ten years, a magnitude directly relevant to municipal decarbonization targets.

These environmental gains are achieved without the land-use trade-offs associated with utility-scale PV, and without requiring any structural modification to the building envelope, making balcony-mounted PV-BESS a low-friction complement to municipal and regional decarbonization strategies for the existing, largely non-retrofittable residential building stock.

4. Conclusions

This study reported a full year (365 consecutive days) of continuously logged operational data from a balcony-mounted PV-BESS system operating in zero feed-in configuration in the Po Valley climate. Over the monitoring period the system generated 1477 kWh of PV energy, achieving an average annual Self-Sufficiency Ratio of 32.34% (rising to 55.8% in summer), while the zero feed-in constraint removed an estimated 289 kWh (16.4%) of the theoretical yield to curtailment. The most significant technical finding, termed here the "Appliance Paradox", showed that the inverter's own standby consumption exceeded the scarce winter PV yield, turning the winter SSR negative (−10.6%) and producing a net grid-consumption penalty rather than a saving during the deepest winter months. The Energy Advantage Index (EAI) introduced in Section 3.6 formalizes this behaviour into a scalable, transferable criterion for predicting the optimal seasonal deactivation window of any small-scale PV-BESS installation, independent of the specific hardware tested here, and, as shown in Section 3.7, doubling as a prospective sizing-validation figure of merit for minimizing or avoiding the Appliance Paradox at the design stage.

Every figure in this study derives from a single system, at a single site, monitored over a single calendar year, so that no claim of statistical generalization across installations, climates or years is made. Neither inter-annual weather variability nor site-to-site differences in shading, orientation or local tariff structures have been captured, which is the principal limitation of the present study. What partly offsets it is the granularity and continuity of the dataset itself: rather than relying on modelled or monthly aggregated estimates, each of the 365 days contributed four independently metered daily quantities—load, PV generation, grid draw, and weather-station-derived theoretical yield—allowing the seasonal patterns reported here, including the counter-intuitive Appliance Paradox, to be identified directly from measurement rather than inferred from simulation. Economically, with a CAPEX of approximately €1100, this single year of data yields a baseline payback period of 4.63 years, a ten-year Return on Investment of approximately 137%, a Net Present Value of €1033 (discounted at 3.6%), and an Internal Rate of Return of 18.49%. Since renewable energy yields vary from one year to the next, this particular year may have been more or less favourable than average. A simple illustrative sensitivity check on this point is reassuring: even under a conservative 10% reduction in annual avoided-grid energy—broadly consistent with the interannual solar resource variability typically observed in temperate European climates—the payback period would extend only marginally, to 5.10 years, with the ten-year ROI remaining above 110%; a more severe 20% shortfall, well beyond what would normally be expected

year-to-year, still leaves a payback period under 5.7 years and a ten-year ROI above 89%. The investment case is therefore not narrowly contingent on the specific weather realized during the monitored year: the underlying economic indicators remain strongly favourable across a wide band of plausible production variability. On this basis, an IRR of 18.49% is a genuinely attractive result for a residential investment of this scale: it comfortably exceeds the returns of government bonds and other capital-guaranteed instruments, and is competitive with the long-run historical returns typically associated with higher-risk asset classes such as public equities [34], while carrying essentially none of their volatility once installed, since the return derives from a fixed avoided energy cost rather than a traded asset price.

Beyond its favourable return profile, the low CAPEX and DIY-level installation simplicity of the plug-and-play PV-BESS architecture leave financial cost and technical complexity as minor barriers to its deployment; as discussed in Section 3.10.1, the main remaining obstacle is instead regulatory—a connection-authorization regime tied to rated inverter power that has not yet been adapted to hardware-enforced zero feed-in systems, which by design cannot inject into the grid regardless of their nominal power class. Future work should extend this single-site, single-year dataset with multi-year monitoring to capture inter-annual weather variability, replicate the experiment across multiple installations and climatic zones to test the generalizability of the Appliance Paradox and the EAI threshold, validate the simulated load profile against metered consumption from real households of varying composition and occupancy pattern, and investigate the EAI at intra-day resolution in combination with short-term solar forecasting to enable pre-emptive rather than purely retrospective deactivation decisions. A complementary line of work, independent of the field site itself, would characterize inverter standby and partial-load conversion losses as a function of output power on a dedicated laboratory testbed, providing manufacturer-independent efficiency curves of the kind assumed in Section 3.7.

Supplementary Materials: The following supporting information can be downloaded at: https://www.mdpi.com/article/10.3390/su182211598/s1, Dataset S1 provides the complete 365-day daily record of the five raw quantities underlying every calculation in this study. The household energy demand (E_{load}) and the energy drawn from the grid (E_{grid}) were each metered by one of the two TONGOU TO-Q-SY1-JWT smart meters described in Section 2.1. The PV energy generated and utilized by the system (E_{PV}) was monitored directly via the inverter's internal telemetry. The Daily Metered Sun Hours (DMSH) were computed as the ratio between E_{PV} and the array's rated peak power, and the Daily Peak Sun Hours (DPSH) were computed by numerically integrating the global horizontal irradiance measured by the weather station's GHI sensor (Section 2.2). The dataset is available as Supplementary Materials: Dataset_S1.xlsx.

Author Contributions: Conceptualization, S.R.; methodology, A.L.; data curation, F.P.; writing—original draft preparation, S.R.; writing—review and editing, G.M.L.; supervision, F.P.; funding acquisition, S.R. All authors have read and agreed to the published version of the manuscript.

Funding: This work has been financed by the Research Fund for the Italian Electrical System (Ministero dell'Ambiente e della Sicurezza Energetica-MASE) under the Three-Year Research Plan 2025–2027 Decree n. 388 of 6 November 2024 "Approvazione del Piano Triennale 2025–2027 della Ricerca di Sistema elettrico", in compliance with the Decree of 12 April 2024, n. 139, grant number B53C22008600001.

Institutional Review Board Statement: Not applicable.

Informed Consent Statement: Not applicable.

Data Availability Statement: The data presented in this study are openly available in the Supplementary Materials (Dataset S1).

Acknowledgments: During the preparation of this manuscript, the authors used Claude AI (Sonnet 5) to check English and correct syntax and to improve the readability of selected passages. The authors have reviewed and edited the output and take full responsibility for the content of this publication.

Conflicts of Interest: The authors declare no conflicts of interest.

Abbreviations

The following abbreviations are used in this manuscript:

AC	Alternating Current
ARERA	Autorità di Regolazione per Energia Reti e Ambiente (Italian Regulatory Authority for Energy, Networks and Environment)
BESS	Battery Energy Storage System
BMS	Battery Management System
CAPEX	Capital Expenditure
CO_2eq	Carbon Dioxide Equivalent
DC	Direct Current
DMSH	Daily Metered Sun Hours
DoD	Depth of Discharge
DPSH	Daily Peak Sun Hours
EAI	Energy Advantage Index
GHI	Global Horizontal Irradiance
IEA	International Energy Agency
IEC	International Electrotechnical Commission
IRR	Internal Rate of Return
ISTAT	Istituto Nazionale di Statistica (Italian National Institute of Statistics)
LCOE	Levelized Cost of Energy
MMSH	Monthly Metered Sun Hours
MPPT	Maximum Power Point Tracking
MPSH	Monthly Peak Sun Hours
PBP	Payback Period
PR	Performance Ratio (IEC 61724)
PV-PR	PV Performance Ratio (array-stage ratio between actual and theoretical solar yield, MMSH/MPSH)
PV	Photovoltaic
PVGIS	Photovoltaic Geographical Information System
ROI	Return on Investment
SOC	State of Charge
SSR	Self-Sufficiency Ratio
STC	Standard Test Conditions

References

1. International Energy Agency (IEA). *Global Energy Review 2025*; IEA: Paris, France, 2025. Available online: https://www.iea.org/reports/global-energy-review-2025 (accessed on 25 September 2026).
2. Bundesnetzagentur. *Growth in Renewable Energy in 2024*; Bundesnetzagentur: Bonn, Germany, 2025. Available online: https://www.bundesnetzagentur.de/SharedDocs/Pressemitteilungen/EN/2025/20250108_EE.html (accessed on 25 September 2026).
3. Gerber, D.L.; Ginsberg-Klemmt, A.; Stoler, L.; Shackelford, J.; Meier, A. Barriers to Balcony Solar and Plug-In Distributed Energy Resources in the United States. *Energies* **2025**, *18*, 2132. [CrossRef]
4. Umweltbundesamt. *Steckersolargeräte Reduzieren Eigene Stromkosten—Auch Für Mieter*innen*; Umweltbundesamt: Dessau-Roßlau, Germany, 2024. Available online: https://www.umweltbundesamt.de/umwelttipps-fuer-den-alltag/heizen-bauen/balkonkraftwerk-steckersolargeraet (accessed on 25 September 2026).
5. Besagni, G.; Premoli Vilà, L.; Borgarello, M. Italian Household Load Profiles: A Monitoring Campaign. *Buildings* **2020**, *10*, 217. [CrossRef]
6. Cheng, X.; Kim, J.; Li, M.; Bae, J. DNA-directed fabrication of $LiFePO_4$ micro-roses as high-performance electrodes for lithium-ion batteries. *Nano Energy* **2025**, *134*, 110577. [CrossRef]
7. Eum, J.; Kim, Y. Analysis on Operation Modes of Residential BESS with Balcony-PV for Apartment Houses in Korea. *Sustainability* **2021**, *13*, 311. [CrossRef]
8. Spaeth, U.; Popp, A.; Fechtner, H.; Cichon, A.; Schmuelling, B. Self-Consumption Optimization of Balcony Solar Systems Using a Load-Controlled Battery Storage. In Proceedings of the 2023 10th International Conference on Power and Energy Systems Engineering (CPESE), Nagoya, Japan, 8–10 September 2023; pp. 378–382.

9. Tan, B.; Liang, Z.; Chung, C.Y.; Dong, H.; Yin, X.; Rayeem, S.K. Uncertainty-Aware Approaches Toward Managing Hydrogen-Powered Vehicles and Renewable Energy Units in Microgrid–Transportation Networks. *IEEE Trans. Transp. Electrif.* **2026**, *12*, 8202–8220. [CrossRef]
10. Polański, J.; Nemś, M.; Michalski, M.; Vassiliades, C. Balcony Photovoltaics in Large-Panel Prefabricated Buildings as a Contribution to the Urban Energy Transition. *Energies* **2025**, *18*, 5789. [CrossRef]
11. Xu, C.; Sun, L.; Rao, Y.; Wu, X.; Liu, Z.; Luo, X. Parametric Modelling for Evaluating Solar Resource Potential and PV/T System Feasibility on Urban Residential Balconies. *Energy Build.* **2026**, *358*, 117209. [CrossRef]
12. Luo, L.; Wu, R. Energy Saving Impact of an Inclined Solar Balcony in a Residential Building. *Iran. J. Chem. Chem. Eng.* **2026**, *45*, 1187–1198. [CrossRef]
13. Stojisavljević, O.; Antić, M. Solar Energy Production in Urban Environments: Integration of Balcony Power Plant into Smart Home Systems. In *Proceedings of the 2026 IEEE Zooming Innovation in Consumer Technologies International Conference (ZINC)*; IEEE: Piscataway, NJ, USA, 2026. [CrossRef]
14. Gögelein, D.; von Schwerin, M. Hierarchical Short-Horizon Model Predictive Control with User Adaptation for Microcontroller-Based Balcony Photovoltaic Energy Management. *IEEE Access* **2026**, *14*, 152848–152867. [CrossRef]
15. Gögelein, D.; von Schwerin, M. Interpretable Predictive Rule-Based Energy Management for Residential Balcony PV Systems with Hybrid Storage. *MATEC Web Conf.* **2026**, *422*, 03006. [CrossRef]
16. Spaeth, U.; Popp, A.; Fechtner, H.; Haack, P. Efficiency Optimization of Balcony Solar Storage Systems: A Parallel Differential Topology Approach. In *Proceedings of the 2026 16th International Conference on Power, Energy, and Electrical Engineering (CPEEE)*; IEEE: Piscataway, NJ, USA, 2026. [CrossRef]
17. Weniger, J.; Tjaden, T.; Bergner, J.; Quaschning, V. Emerging Performance Issues of Photovoltaic Battery Systems. In Proceedings of the 32nd European Photovoltaic Solar Energy Conference and Exhibition (EU PVSEC), Munich, Germany, 20–24 June 2016. [CrossRef]
18. ARPAE (Agenzia Regionale per la Prevenzione, l'Ambiente e l'Energia dell'Emilia-Romagna). *Dext3r—Estrazione Dati Meteo*; ARPAE: Bologna, Italy. Available online: https://simc.arpae.it/dext3r/ (accessed on 8 October 2026).
19. Jinko Solar Co., Ltd. *Tiger Neo N-Type 54HL4R-(V) 435-460 Watt Datasheet*; Jinko Solar: Shanghai, China, 2024.
20. European Commission, Joint Research Centre. Photovoltaic Geographical Information System (PVGIS). Available online: https://re.jrc.ec.europa.eu/pvg_tools/en/ (accessed on 29 September 2026).
21. Khalid, A.M.; Mitra, I.; Warmuth, W.; Schacht, V. Performance ratio—Crucial parameter for grid connected PV plants. *Renew. Sustain. Energy Rev.* **2016**, *65*, 1139–1158. [CrossRef]
22. Wassie, Y.T.; Ahlgren, E.O. Performance and reliability analysis of an off-grid PV mini-grid system in rural tropical Africa: A case study in southern Ethiopia. *Dev. Eng.* **2023**, *8*, 100106. [CrossRef]
23. ARERA (Autorità di Regolazione per Energia Reti e Ambiente). *Relazione Annuale 2026*; ARERA: Milan, Italy, 2026.
24. *IEC 61683:1999*; Photovoltaic Systems—Power Conditioners—Procedure for Measuring Efficiency. International Electrotechnical Commission: Geneva, Switzerland, 1999.
25. Anern (Guangzhou Anern Energy Technology Co., Ltd.). *ECO-6200 Hybrid Inverter Datasheet*; Anern: Guangzhou, China, 2024.
26. Meissner, L. *Energy Storage Behind the Data Sheet*; HTW Berlin: Berlin, Germany, 2024. Available online: https://solar.htw-berlin.de/wp-content/uploads/MEISSNER-2024-Energy-storage-behind-the-data-sheet.pdf (accessed on 29 September 2026).
27. ISTAT (Istituto Nazionale di Statistica). *Prezzi al Consumo, Dati Definitivi, Dicembre 2021–2025 (Annual Average Inflation Rates)*; ISTAT: Rome, Italy. Available online: https://www.istat.it/ (accessed on 30 October 2026).
28. Naumann, M.; Spingler, F.B.; Jossen, A. Analysis and Modeling of Cycle Aging of a Commercial $LiFePO_4$/Graphite Cell. *J. Power Sources* **2020**, *451*, 227666. [CrossRef]
29. Rauhala, T.; Jalkanen, K.; Romann, T.; Lust, E.; Omar, N.; Kallio, T. Low-Temperature Aging Mechanisms of Commercial Graphite/$LiFePO_4$ Cells Cycled with a Simulated Electric Vehicle Load Profile—A Post-Mortem Study. *J. Energy Storage* **2018**, *20*, 344–356. [CrossRef]
30. ARERA (Autorità di Regolazione per Energia Reti e Ambiente). *Testo Integrato Autoconsumo Diffuso (TIAD)*; Delibera 727/2022/R/eel; ARERA: Milan, Italy, 2022.
31. ISPRA. *Fattori di Emissione Atmosferica di CO_2 e Altri Gas a Effetto Serra Nel Settore Elettrico*; ISPRA: Rome, Italy, 2024.
32. ACEA. *The Automobile Industry Pocket Guide 2023/2024*; ACEA: Brussels, Belgium, 2023.
33. Mazon, J. Integrating Urban Tree Carbon Sequestration into Metropolitan Ecosystem Services for Climate-Neutral Cities: A Citizen Science-Based Methodology. *Urban Sci.* **2025**, *9*, 463. [CrossRef]
34. Dimson, E.; Marsh, P.; Staunton, M. *UBS Global Investment Returns Yearbook 2025*; UBS: Zurich, Switzerland, 2025.

Disclaimer/Publisher's Note: The statements, opinions and data contained in all publications are solely those of the individual author(s) and contributor(s) and not of MDPI and/or the editor(s). MDPI and/or the editor(s) disclaim responsibility for any injury to people or property resulting from any ideas, methods, instructions or products referred to in the content.